RESEARCH ARTICLE | AUGUST 05 2024

Development of a measuring technique based on JET second D-T campaign (DTE2) experience for assessing fusion power at ITER during D-T operation using the radial gamma-ray spectrometer

Special Collection: Proceedings of the 25th Topical Conference on High-Temperature Plasma Diagnostics

G. Marcer ; F. Scioscioli ; G. Croci ; A. Dal Molin ; G. Gorini ; A. Muraro ; M. Nocente ; E. Perelli Cippo ; M. Rebai ; D. Rigamonti ; B. Coriton ; A. Kovalev ; A. Polevoi ; E. Khilkevitch ; A. Shevelev ; A. Bracco; F. Camera; C. Cazzaniga ; M. Tardocchi

Rev. Sci. Instrum. 95, 083515 (2024)
https://doi.org/10.1063/5.0217677

Review of Scientific Instruments ARTICLE pubs.aip.org/aip/rsi

Development of a measuring technique based on JET second D-T campaign (DTE2) experience for assessing fusion power at ITER during D-T operation using the radial gamma-ray spectrometer

Cite as: Rev. Sci. Instrum. 95, 083515 (2024); doi: 10.1063/5.0217677
Submitted: 6 May 2024 • Accepted: 13 July 2024 •
Published Online: 5 August 2024

G. Marcer,[1,a] F. Scioscioli,[1,2] G. Croci,[1] A. Dal Molin,[2] G. Gorini,[1,2] A. Muraro,[2] M. Nocente,[1,2] E. Perelli Cippo,[2] M. Rebai,[2] D. Rigamonti,[2] B. Coriton,[3] A. Kovalev,[3] A. Polevoi,[3] E. Khilkevitch,[4] A. Shevelev,[4] A. Bracco,[5] F. Camera,[5] C. Cazzaniga,[6] and M. Tardocchi[2]

AFFILIATIONS

[1] Department of Physics, University of Milan-Bicocca, Milan, Italy
[2] Institute for Plasma Science and Technology, CNR, Milan, Italy
[3] Diagnostic Program, ITER Organization, Saint Paul-lez-Durance, France
[4] Independent researcher, St. Petersburg, Russian Federation
[5] Department of Physics, University of Milan, Milan, Italy
[6] UKRI-STFC, Rutherford Appleton Laboratory, Didcot, United Kingdom

Note: This paper is part of the Special Topic on Proceedings of the 25th Topical Conference on High-Temperature Plasma Diagnostics.

[a] **Author to whom correspondence should be addressed:** g.marcer@campus.unimib.it

ABSTRACT

The ITER Radial Gamma-Ray Spectrometer (RGRS) consists of three gamma-ray detectors observing the plasma through three collimated, coplanar, radial lines of sight (LoS). The system was initially designed to monitor the runaway electron emission and the alpha-particle density profile [Nocente et al., Nucl. Fusion **57**, 076016 (2017)]. This work presents a novel technique for measuring the fusion power during D-T operation using the RGRS. This method is based on the absolute measurement of the 17 MeV fusion gamma-rays and a semi-analytical computation of their transport from the plasma source to the detectors. This approach was initially developed and tested at JET during the second D-T campaign (DTE2) on a single LoS diagnostic [Dal Molin *et al.*, Phys. Rev. Lett. (submitted) (2024); Rebai *et al.*, Phys. Rev. C (submitted) (2024); and Marcer *et al.*, Nucl. Fusion (unpublished) (2024)]. This work exploits the multiple LoS of the RGRS to create a combined virtual diagnostic whose detected fraction of the total plasma emission is less affected by variations in the plasma emission profile, reducing systematic uncertainties on the estimated total emission, compared to the individual detectors.

I. INTRODUCTION

The tokamaká ITER endeavors to become the first large-size magnetic confined fusion device to achieve a net energy gain from nuclear fusion reactions. The highest fusion power output will be reached during D-T experiments, when the diagnostics for measuring fusion power will have to provide accurate and reliable results.

Among other systems, ITER will be equipped with the radial gamma-ray spectrometer (RGRS),[1] whose main role will be to mea-

sure the runaway electron distribution and the alpha particle density profile. This work presents a novel technique for measuring the fusion power at ITER during D-T operation using the RGRS.

This method relies on the absolute measurement of the 17 MeV gamma-rays emitted by the secondary radiative channel of the D-T fusion reaction,

$$\mathrm{D} + \mathrm{T} \rightarrow {}^{5}\mathrm{He}^{*} \rightarrow \begin{cases} {}^{4}\mathrm{He} + \mathrm{n}, & \mathrm{BR} \sim 1, \\ {}^{5}\mathrm{He} + \gamma, & \mathrm{BR} = 2.4 \cdot 10^{-5}, \end{cases}$$

which is considerably less probable compared to the primary neutronic branch.[2,3] Being the neutron emission about 10^5 times more abundant, gamma-ray measurements with the RGRS will require the use of LiH neutron attenuators in order to minimize the unwanted neutron interactions with the detectors.[5]

The RGRS consists of three detectors observing the plasma through three collimated Lines of Sight (LoS). When dealing with collimated LoS for absolute measurements, the relationship between the actual measurements and the overall radiation emission heavily depends on the Fraction of the Observed Plasma Emission (FOPE). In this study, the FOPE was characterized for the RGRS with a semi-analytical computation of the detectors' transport probability matrices.

This approach was developed and tested at JET during the second deuterium–tritium experimental campaign (DTE2)[6–8] for a single LoS diagnostic.[4] The plurality of LoS in the RGRS allows for tracking the position of the plasma inside the vessel. In this study, it was leveraged to create a combined diagnostic whose FOPE is less affected by variations in the plasma emission profile compared to the individual detectors, thereby reducing reliance on neutron profile measurements to enhance the accuracy of fusion power determination. In principle, information on plasma emission profiles could be provided by other diagnostics, further improving the RGRS fusion power assessment performance.

This paper is structured as follows: Section II elucidates the measurement of fusion power in a D-T plasma using a single LoS gamma-ray diagnostic. Section III delineates the RGRS geometry and transport probability matrices. Section IV outlines the conceptual utilization of its multiple LoS, while the algorithm employed is detailed in Sec. V. Finally, Sec. VI presents the conclusions.

II. FUSION POWER MEASUREMENT

In a tokamak, the fusion power is usually measured with standard techniques, which rely on the absolute measurement of the 14 MeV neutrons emitted by the main channel of the D-T reaction. At JET, the measurements were performed with three fission chambers located around the tokamak in the torus hall. Data were interpreted based on massive numerical simulations of neutron transport in the tokamak and cross-calibrated with activation foils, leading to a nominal overall uncertainty of 7% on the provided fusion power.[9]

The method was developed and tested at JET during the DTE2 campaign, utilizing the tangential gamma-ray spectrometer for this purpose.[8] The detector was positioned ~23 m outside the vessel, at the end of a collimated, horizontal line of sight. The method, detailed in Ref. 4, necessitates careful characterization of gamma-ray transport from the plasma source to the detector. Since gamma-rays have a much higher probability of attenuation compared to neutrons, an optical description of their transport is possible, which is much simpler than the complex neutron transport calculations through all tokamak surrounding material. Information about gamma-ray transmittance through the collimators can then be obtained with dedicated simulations.

As mentioned earlier, the plasma emission profile plays a crucial role in measuring fusion power using the GET-ART method. Due to the collimated lines of sight, the transport of gamma-rays heavily relies on the plasma's position within the chamber and its D-T gamma-ray emission profile. To address this challenge, a semi-analytical code named Linalytic was specifically developed. Linalytic calculates the probability that a particle originating from a specific point inside the vessel will reach the detector's front face. This calculation assumes that there are no attenuating objects along the line of sight and that all other objects are completely opaque, following an optical transport model. Linalytic was employed to compute these probabilities for a poloidal section of ITER, averaging the probabilities along the toroidal direction to create a matrix of pixels. Each pixel in the poloidal plane corresponds to a transport probability, resulting in a transport probability matrix.

III. DETECTORS' GEOMETRY AND TRANSPORT PROBABILITY MATRICES

The RGRS will consist of three detectors observing the plasma through three radial, coplanar, collimated lines of sight, positioned ~18 m from the torus center. The lines of sight intersect each other outside the vessel, with the upper detector having the lower line of sight inside the vessel, and vice versa. Once inside the vessel, all lines of sight are above the equatorial plane. A fourth channel is also part of the RGRS but was not included in the analysis due to the presence of other diagnostics along the detector beamline, which would pose challenges for absolute measurements with this detector.

Each detector will comprise a cylindrical scintillating lanthanum bromide crystal coupled to a photomultiplier tube.[10] The LoS will feature a conical aperture, resulting in a normal section area of ~100 cm^2 at the central column.

The transport probability matrices for the detectors inside the vessel were computed using Linalytic and are depicted in Fig. 1. As mentioned earlier, for the ith pixel, the transport probability matrix represents the probability p_i for a particle born at that (R, Z) position to reach the detector front face.

The transport probability matrix is to be used together with information about the plasma emission profile in order to assess the FOPE. For each D-T plasma scenario planned for ITER, the fusion gamma-ray emission profile has been simulated. Each plasma discharge entails the ramp-up, flat-top, and ramp-down phases. Since fusion power is produced throughout the whole discharge and not only during the stationary flat-top operation, marked differences are expected in the FOPE, due to differences in location and spatial extension of the emission profile. For the purposes of this work, the simulated emission profiles were computed in the same pixels of the transport probability matrix matrices, leading to the examples shown in Fig. 2. In these plots, each pixel represents the neutron rate e_i generated by the associated toroidal voxel.

The transport probability matrix is utilized in conjunction with information about the plasma emission profile to evaluate the FOPE.

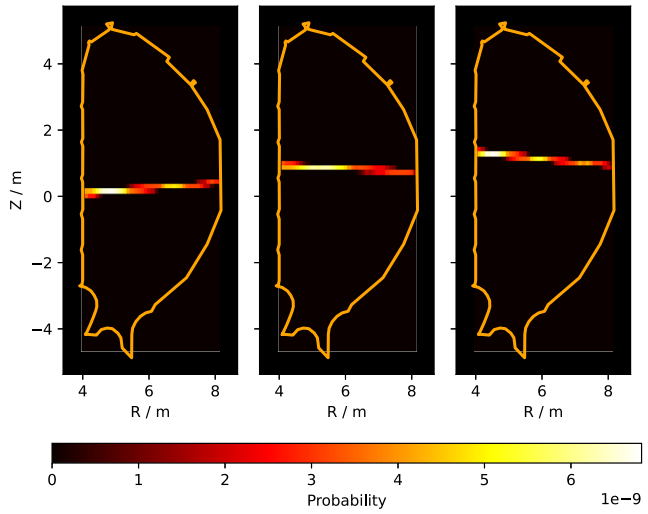

FIG. 1. RGRS detectors' transport probability matrices computed with Linalytic. Detectors are numbered from 1 to 3 from left to right.

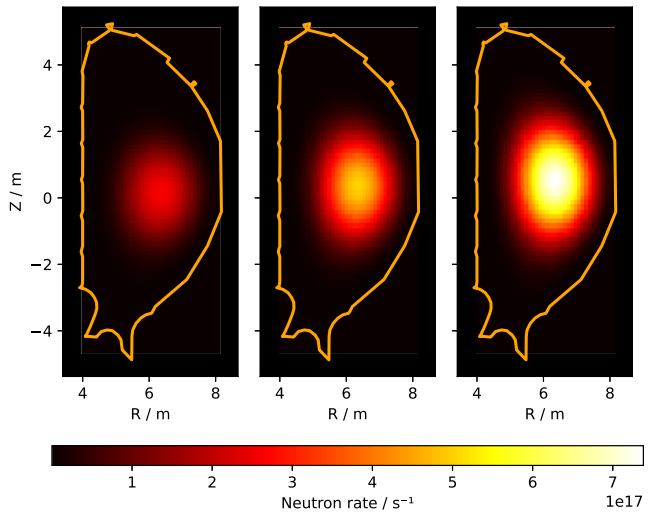

FIG. 2. Example of ITER D-T plasma emission profiles during a discharge ramp-up. Increasing time from left to right. Data were taken from the IMAS database.

For each planned D-T plasma scenario in ITER, the fusion gamma-ray emission profile has been simulated. Each plasma discharge comprises the ramp-up, flat-top, and ramp-down phases. As fusion power is generated throughout the entire discharge and not solely during the stationary flat-top operation, significant differences are anticipated in the FOPE, attributed to variations in the location and spatial extent of the emission profile during ramp plasmas. For this study, the simulated emission profiles were computed within the same pixels of the transport probability matrices, resulting in the examples depicted in Fig. 2. In these plots, each pixel represents the neutron rate e_i generated by the corresponding toroidal voxel.

With the emissivity e_i of each pixel at hand, the FOPE T for each emission profile was computed as the emission-weighted average of all probabilities,

$$T = \frac{\sum_i e_i V_i p_i}{\sum_i V_i e_i},$$

where i runs over all pixels and V_i is the volume associated with the ith pixel, when the toroidal dimension is also taken into account. Such a computed probability was found to be about 1.2×10^{-10} for all profiles.

IV. CONCEPTUAL MEASURING TECHNIQUE

The aim of this work was to combine the RGRS detectors to create a virtual diagnostic with the best possible accuracy in measuring fusion power, even without information about the plasma emission profiles. This involved devising a method to combine the RGRS detectors to produce a virtual detector whose FOPE remains as constant as possible when computed for different plasma emission profiles.

The virtual detector was developed using data obtained from the ITER Integrated Modeling and Analysis System (IMAS).[11] A set of 32 emission profiles was utilized for this study, with 13 related to flat-top operations and 19 to ramp plasmas. A constraint was imposed on the total neutron rate to be at least 10^{18} neutrons per second (~3 MW of fusion power), corresponding to the lower threshold required for ITER machine-protection diagnostics.

For each ith profile and dth detector, the FOPE T_d^i was computed with Linalytic, with $d \in \{1, 2, 3\}$ (Fig. 1). Then, for each detector, the mean over the profiles $\langle T_d \rangle$ was computed and the percentage relative deviation ΔT_d^i was computed for each profile as

$$\Delta T_d^i = \left(100 \cdot \frac{|T_d^i - \langle T_d \rangle|}{\langle T_d \rangle} \right).$$

The maximum deviations are shown in Table I depending on the considered set of scenarios.

In particular, if the average value were used as a fixed FOPE value during real plasma operations, the discrepancy between this average and the true FOPE of each specific discharge would affect the total gamma-ray emissivity and, consequently, the fusion power. In Fig. 3, the two plots above and the one below on the left show the deviation of the FOPEs' average from the true values for each detector, based on the entire set of employed IMAS profiles. The three detectors exhibit comparable results, with detector 2 showing

TABLE I. Maximum percentage deviation of the FOPEs from their mean for each detector. The profiles are divided into sets based on the employed profile plasma operation.

	Flat-top	Ramp	Both
d_1	18.37	13.40	21.99
d_2	18.35	7.89	19.46
d_3	15.65	15.28	15.66

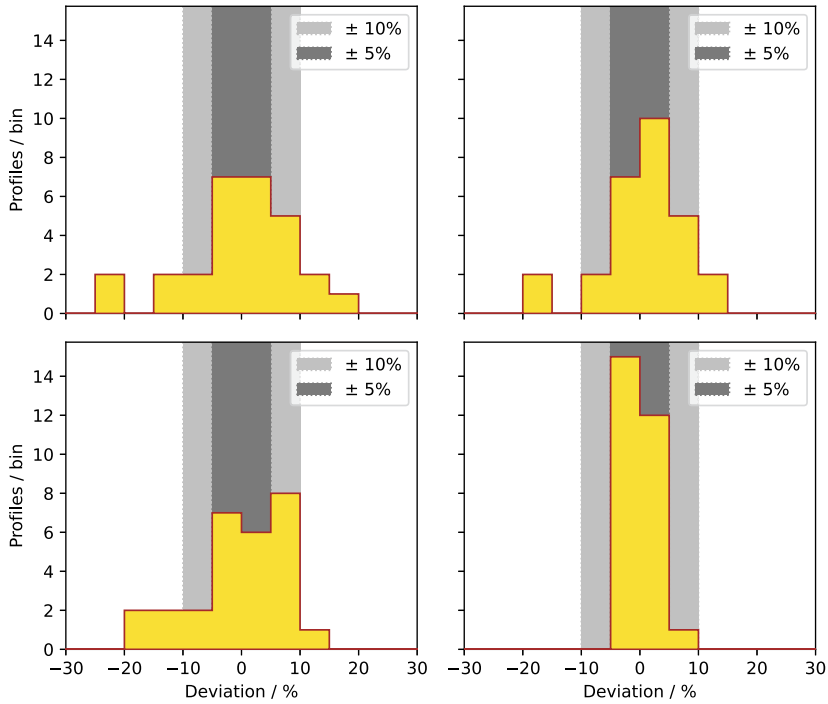

FIG. 3. Percentage deviations of the measured fusion power from the true value when estimated with single detectors (d_1 upper left plot, d_2 upper right plot, d_3 lower left plot, virtual detector lower right plot) with the entire profiles' dataset.

the least variation during ramp plasma operations due to its proximity to the magnetic axis and detector 3 having the most stable FOPE overall.

The results in Fig. 3 suggest that the FOPE of the three detectors may be combined linearly with suitable weights to obtain an overall FOPE for the virtual detector that is less prone to changes in the emission profile. Let us define the virtual detector FOPE as

$$T_{\text{virtual}} = a_1 T_1 + a_2 T_2 + a_3 T_3.$$

The weights a_1, a_2, and a_3 were determined through a minimization algorithm described in Sec. V. In order to avoid the trivial solution $a_1 = a_2 = a_3 = 0$, a constraint was imposed on the weights,

$$a_1 + a_2 + a_3 = 1 \quad \rightarrow \quad a_1 = 1 - a_2 - a_3,$$

which leads to

$$T_{\text{virtual}} = T_1 + a_2(T_2 - T_1) + a_3(T_3 - T_1).$$

Written in this form, the virtual detector depends on the absolute value of T_1 and, through the weights a_2 and a_3, on the differences between the FOPE of the first detector and those of the other two detectors.

The virtual detector still depends on the true FOPEs, and its average value $\langle T_{\text{virtual}} \rangle$ could be used during plasma operations. Compared to the single detectors, the virtual detector shows a much lower FOPE variation depending on the plasma emission profiles as shown in Table II and in the last plot of Fig. 3 (for both flat-top and ramp-up/down plasma scenarios). In particular, all profiles but one fall within ±5% discrepancy.

The best coefficients were found to be $a_1 = 1.883$, $a_2 = -4.671$, $a_3 = 3.778$ and $T = 1.169 \times 10^{-10}$, the last corresponding to the average FOPE of all used profiles. These values indicate that the virtual FOPE scales linearly with the FOPE of the first and third detectors,

TABLE II. Maximum percentage deviation of the FOPEs from their mean for the virtual detector. The profiles are divided into sets based on the employed profile plasma operation.

	Flat-top	Ramp	Both
Virtual det.	6.42	2.52	5.62

TABLE III. Comparison between the training set and the test set for both the single detectors and the virtual detector: maximum percentage deviation of the FOPEs from their mean.

	Training set	Test set
d_1	21.99	21.50
d_2	19.46	19.99
d_3	15.66	16.80
Virtual det.	5.62	6.38

while varying inversely with respect to the central one. This could be interpreted as an attempt to reduce variations due to the peaking of the plasma profile, rather than shifts of the profile itself.

These virtual detector parameters were tested with an additional set of 51 IMAS profiles to verify the output stability. Table III shows the resulting maximum percentage deviations for this new set of scenarios, confirming that the virtual detector performs as expected.

V. OPTIMIZATION ALGORITHM

The purpose of the virtual detector is to reduce the discrepancy between the fusion power measurement with respect to the true value during plasma operations, when no information is provided about the plasma emission profile. This requires finding properly optimized weights for the detectors' transport factors. The best parameters were found using the same set of plasma profiles from the IMAS database used so far.

For the single ith profile, the detectors' transports T_1^i, T_2^i, and T_3^i were estimated with Linalytic and their linear combination is computed as

$$T^i(a_2, a_3) = T_1^i + a_2(T_2^i - T_1^i) + a_3(T_3^i - T_1^i).$$

The number of virtual FOPEs, therefore, corresponds to the number of profiles at disposal. It was then required for them to be as close as possible to a constant T by minimizing the following function:

$$f(a_2, a_3, T) = \sum_i \left(T - T^i(a_2, a_3)\right)^2.$$

We emphasize that determining the constant T is part of the optimization procedure. The analytic solution found with three reference plasma emission profiles was employed as the initial guess of the minimization algorithm,

$$\begin{cases} T - T_1^1 + a_2(T_2^1 - T_1^1) + a_3(T_3^1 - T_1^1) = 0, \\ T - T_1^2 + a_2(T_2^2 - T_1^2) + a_3(T_3^2 - T_1^2) = 0, \\ T - T_1^3 + a_2(T_2^3 - T_1^3) + a_3(T_3^3 - T_1^3) = 0. \end{cases}$$

An example of the parameter minimization space is shown in Fig. 4. As can be observed, there is only one local minimum within the checked parameter ranges. Specifically, the limits of the constant T were chosen in an interval spanning two decades centered around the absolute value of the single transports T_i (10^{-10}).

The minimization algorithm is equivalent to the minimization of the variance of the virtual detector FOPE, once both single detector variances and covariances are taken into account. This explains why the optimal parameter T corresponds to the linear combination of the mean values of the individual detector FOPEs.

VI. CONCLUSIONS

The tokamak ITER will be equipped with a radial gamma-ray spectrometer (RGRS) for monitoring the distribution of runaway electrons and the alpha particle profile. This study investigated the feasibility of also using the RGRS to measure the fusion power in D-T plasmas producing at least 3 MW of fusion power.

The measurement technique developed at JET during the second deuterium–tritium campaign (DTE2) was optimized for the RGRS, focusing on the optical transport of gamma-rays from the plasma to the detector. The plurality of lines of sight (LoS) in the RGRS was leveraged to build a virtual diagnostic with better accuracy compared to a single LoS, particularly in the absence of external information on the plasma D-T emission profile. It was found that the accuracy of fusion power measurement could be improved from ~20% down to around 5.6% by suitably combining the data from the three RGRS detectors.

These results support the additional use of the RGRS for fusion power measurements at ITER.

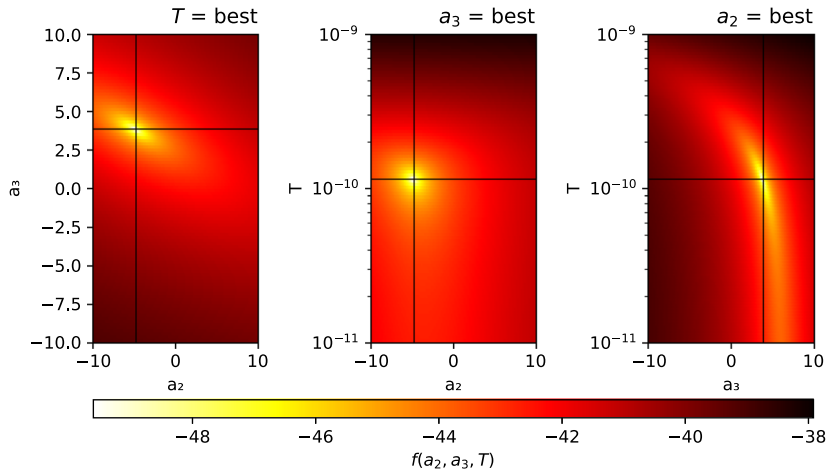

FIG. 4. Function f minimization. The parameter space is shown in three two-dimensional plots, keeping fixed one parameter at a time, equal to the best parameter. In each plot, the solution is shown with the black lines.

VII. DISCLAIMER

The views and opinions expressed here do not necessarily reflect those of the ITER Organization.

AUTHOR DECLARATIONS

Conflict of Interest

The authors have no conflicts to disclose.

Author Contributions

G. Marcer: Conceptualization (equal); Data curation (lead); Formal analysis (lead); Investigation (lead); Methodology (equal); Software (lead); Validation (equal); Visualization (lead); Writing – original draft (lead). **F. Scioscioli**: Conceptualization (equal); Methodology (equal); Supervision (equal); Writing – review & editing (equal). **G. Croci**: Conceptualization (equal); Funding acquisition (lead); Methodology (equal); Project administration (lead); Resources (lead); Supervision (equal); Writing – review & editing (supporting). **A. Dal Molin**: Conceptualization (supporting); Data curation (supporting); Formal analysis (supporting); Methodology (supporting); Supervision (supporting); Validation (supporting); Writing – review & editing (supporting). **G. Gorini**: Funding acquisition (equal); Resources (equal). **A. Muraro**: Conceptualization (equal); Methodology (equal). **M. Nocente**: Supervision (supporting); Validation (supporting); Writing – review & editing (lead). **E. Perelli Cippo**: Conceptualization (supporting); Methodology (supporting); Supervision (supporting). **M. Rebai**: Conceptualization (supporting); Funding acquisition (lead); Project administration (lead); Resources (lead); Supervision (supporting). **D. Rigamonti**: Methodology (supporting); Supervision (supporting); Validation (supporting). **B. Coriton**: Funding acquisition (lead); Project administration (equal); Resources (lead); Supervision (supporting); Validation (supporting). **A. Kovalev**: Data curation (equal); Formal analysis (equal); Funding acquisition (supporting); Investigation (equal); Methodology (equal); Project administration (equal); Resources (supporting); Software (supporting); Supervision (lead); Validation (supporting). **A. Polevoi**: Data curation (equal); Resources (equal); Supervision (supporting). **E. Khilkevitch**: Conceptualization (supporting); Methodology (supporting). **A. Shevelev**: Conceptualization (supporting); Methodology (supporting). **A. Bracco**: Supervision (supporting); Validation (supporting). **F. Camera**: Supervision (supporting); Validation (supporting). **C. Cazzaniga**: Conceptualization (supporting); Methodology (supporting); Writing – review & editing (supporting). **M. Tardocchi**: Conceptualization (supporting); Formal analysis (supporting); Funding acquisition (supporting); Investigation (supporting); Methodology (supporting); Project administration (supporting); Supervision (equal); Validation (equal); Writing – review & editing (supporting).

DATA AVAILABILITY

The data that support the findings of this study are available from the corresponding author upon reasonable request.

REFERENCES

[1] M. Nocente *et al.*, Nucl. Fusion **57**, 076016 (2017).
[2] A. Dal Molin *et al.*, "Measurement of the gamma ray to neutron branching ratio for the deuterium-tritium reaction in magnetic confinement fusion plasmas," Phys. Rev. Lett. (to be published) (2024).
[3] M. Rebai *et al.*, "First direct measurement of the spectrum emitted by the ^{3}H(^{2}H, γ)^{5}He reaction and assessment of the γ_0 and γ_1 relative yield," Phys. Rev. C (to be published) (2024).
[4] G. Marcer *et al.*, "Measurement of the DT reaction gamma-ray emission in magnetic confinement fusion plasmas," (unpublished) (2024).
[5] D. Rigamonti *et al.*, Rev. Sci. Instrum. **93**, 093515 (2022).
[6] J. Mailloux *et al.*, Nucl. Fusion **62**, 042026 (2022).
[7] M. Nocente *et al.*, Rev. Sci. Instrum. **93**, 093520 (2022).
[8] M. Nocente *et al.*, Rev. Sci. Instrum. **92**, 053529 (2021).
[9] D. B. Syme *et al.*, Fusion Eng. Des. **89**, 2766 (2014).
[10] M. Nocente *et al.*, IEEE Trans. Nucl. Sci. **60**, 1408 (2013).
[11] L. Kos *et al.*, in NENE 2017, 2017.